ACS APPLIED MATERIALS & INTERFACES

Letter

www.acsami.org

Field Emission from Hybrid Diamond-like Carbon and Carbon Nanotube Composite Structures

H. Zanin,*[,†] P. W. May,[†] M. H. M. O. Hamanaka,[‡] and E. J. Corat[§]

[†]School of Chemistry, University of Bristol, Bristol BS8 1TS, United Kingdom

[‡]Information Display Division, Centre for Information Technology Renato Archer, Rod. Dom Pedro I km 143, Campinas 13069-901, São Paulo, Brazil

[§]National Institute for Space Research, Av. dos Astronautas 1758, São Jose dos Campos, 12227-010, São Paulo, Brazil

Supporting Information

ABSTRACT: A thin diamond-like carbon (DLC) film was deposited onto a densely packed "forest" of vertically aligned multiwalled carbon nanotubes (VACNT). DLC deposition caused the tips of the CNTs to clump together to form a microstructured surface. Field-emission tests of this new composite material show the typical low threshold voltages for carbon nanotube structures (2 V μm^{-1}) but with greatly increased emission current, better stability, and longer lifetime.

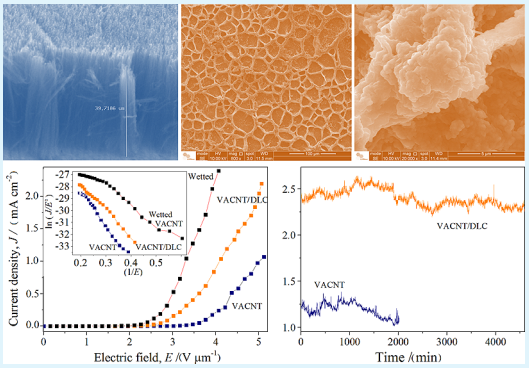

KEYWORDS: *field emission, carbon−carbon composite, porous DLC, low threshold voltage, aligned nanotubes, DLC*

1. INTRODUCTION

Carbon-based materials are suitable for use as cold cathode emitters because of the low voltages required for extraction of electrons. Thin carbon films with low threshold fields can give emission current densities high enough for use in flat panel displays,[1,2] and X-ray[3] and microwave generators.[4] A wide range of carbon-based field emitters, such as doped diamond, diamond-like carbon and carbon nanotubes (CNTs), have been extensively studied. Field-emission current densities of up to 1 mA cm^{-2} were observed for applied electric fields of less than 5 V μm^{-1}.[5] However, poor uniformity and low current stability have hindered further commercial development.[2,6]

Field-emission efficiency is determined by a combination of factors, including the conductivity of the emitter, the surface work function, the resistance of the emitter/substrate interface, and the sharpness of the emitting tip (which controls the field-enhancement factor, β).[7] An ideal field emitter should be a good electrical conductor with low work function, high enhancement factor and be stable at high emission current density. Boron-doped diamond has excellent conductivity and a robust surface with a low work function, allowing some excellent field-emission devices to be constructed.[8,9] However, to obtain a high β value, complex and expensive micro-fabrication is usually required to pattern and etch the diamond into suitable pyramids or needle shapes, although recently diamond nanocones have been made using a single-step CVD process that show promising field-emission characteristics.[10] Conversely, CNTs have a nanosharp tip as well as high electrical conductivity, and can be prepared as vertically aligned (VA) structures, or dense "forests".[7] These have excellent field-emission properties, with currents of 1 mA cm^{-2} reported for threshold fields as low as 2 V μm^{-1}.[4] However, their sensitivity to slight air (oxygen) leaks into the vacuum system, combined with their tendency to burn out has made their use in field-emission problematic. Often the problem is that the tallest CNT in the forest experiences the highest field and so emits the entire current, which causes it to burn out. The emission then jumps to the next tallest CNT, which survives for a time, then also burns out. Gradually, one by one, the CNT forest is burnt out, until emission ceases completely.

One approach to solve this problem is to use bundles of CNTs to form a dense matrix of close-packed CNTs, which usually join together in a nonaligned, random arrangement. The resulting macroscopic fiber bundles allow the emission current to be shared among many CNTs, providing low threshold fields and hence increased lifetime and durability. Indeed, such CNT bundles have recently been reported to have threshold field as low as 0.12 V μm^{-1} and very high current densities of the order of 13 A cm^{-2}, with lifetimes measured up to 30 h with high stability.[11] Such macroscopic fibres show great promise for single-source electron beams, but for multisource microscale devices the task of assembling these

Received: August 14, 2013
Accepted: November 13, 2013
Published: November 13, 2013

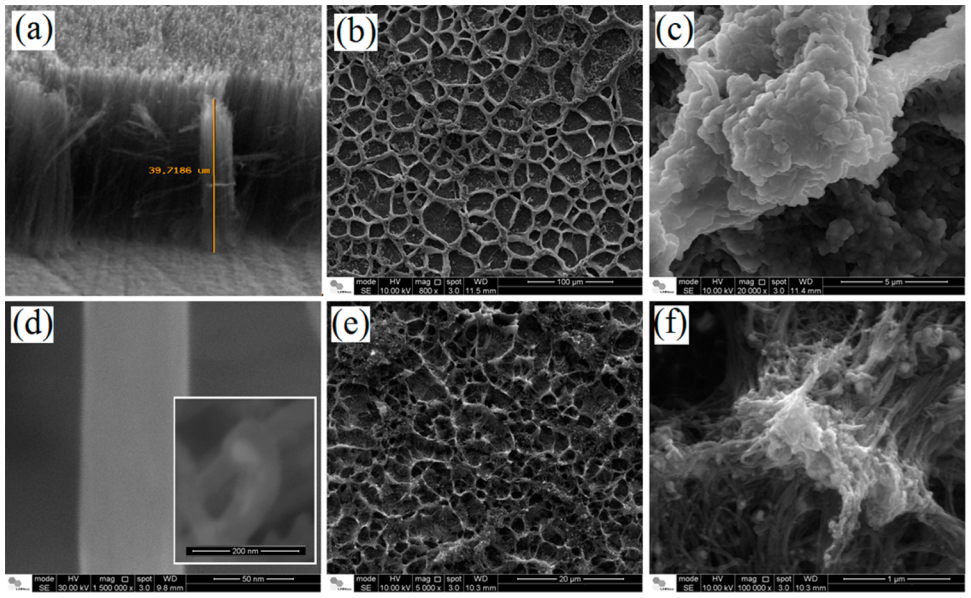

Figure 1. Electron microscope images of the sample morphologies: (a) the as-grown VACNT forest. (b) Top view of VACNT/DLC composite showing the honeycomb structures. (c) Higher-magnification image of the DLC coating on top of the VACNT/DLC honeycomb ridges. (d) Transmission electron microscope images of the as-grown VACNT and (inset) the VACNT/DLC, allowing the CNT diameter before and after DLC deposition to be estimated. (e) Top view of VACNT samples following immersion in water and drying. (f) Detail of the agglomeration at the tips of the joined structures following wetting.

CNT cathode bundles onto a predefined pattern would be quite challenging.

Other attempts to improve the field-emission behavior of CNTs often involve combining the current-carrying properties of CNTs with a modification to the emitting surface. For example, CNTs have been decorated with nanoparticles of erbium,[12] silver,[13] and ZnO,[14] all of which improved the emission characteristics slightly. Several groups have coated CNTs with nanodiamond, either individually,[14,15] as a dense bundle or mat,[16] or as clusters.[2] The robust nature of the nanodiamond surface often imparted excellent field-emission properties on the CNTs, with low threshold fields and high currents while maintaining high enhancement factors. However, the individually coated CNTs often still suffered from low lifetimes because of sequential burn out, as mentioned earlier.

Zou et al.[8] recently showed that by electrospraying a multiwalled VACNT forest with a nanodiamond-in-liquid suspension, the liquid surface tension caused the tips of the CNTs to stick together to form what the authors termed "teepee" structures. The teepees were composed of ∼50 CNTs meeting at a common point. Subsequent short diamond deposition allowed a thin layer of boron-doped diamond to be grown onto these teepees, locking the structure in place. Field-emission tests showed that although the threshold voltages were similar to those from normal B-doped diamond, the stability of the emission was greatly improved, as was the lifetime, which exceeded a few thousand hours even at relatively high emission currents. These structures combined the high current carrying capacity of the ∼50 component CNTs with the robust low-work-function of the emitting diamond surface to produce a composite field-emission material that has the electrical characteristics and long lifetime required for commercial devices.

However, diamond chemical vapor deposition (CVD) is still a relatively expensive and manpower intensive procedure, and for coating the teepees the growth time had to be carefully controlled to obtain optimal results. An alternative approach is to use diamond-like carbon (DLC) as the capping layer for the teepee structures. DLC is a type of amorphous carbon film with high sp^3 carbon content that can be deposited using CVD techniques over large areas at low temperatures,[1,17] and this has now become a relatively cheap, widespread industrial process. Moreover, DLC is another strong candidate for field-emission cathode devices because of its low electron affinity and chemical inertness. The field-emission properties of DLC depend upon the thickness, density, microstructure and sp^2/sp^3 carbon ratio in the films,[1,18,19] with typical threshold field values ranging from 5 to 50 V μm^{-1}.[1,7,20−22] These values are not as low as those for CNTs or diamond, but DLC has the advantage of simplicity of deposition and scalability to large area.

In this work, we study for the first time the field-emission properties of VACNT/DLC composite materials. Thin DLC films were deposited onto dense VACNT forests creating a 3D microstructure as a result of the CNT tips sticking together. We evaluate this new material using scanning electron microscopy, Raman spectroscopy, and field-emission tests.

2. EXPERIMENTAL SECTION

The VACNT films were produced using a microwave-plasma (MWCVD) chamber operating at 2.45 GHz.[23] Substrates were Ti sheets (10 mm × 10 mm × 0.5 mm) covered with a 10 nm Ni layer deposited by electron-beam evaporation. The Ni layer was heated in a N_2/H_2 (10/90 sccm) plasma, which caused it to ball up into nanoclusters that subsequently became the catalyst particles for VACNT growth. The nanocluster formation took place as the substrate temperature increased from 350 to 800 °C over a period of 5 min. To grow the VACNT forest, we introduced CH_4 (14 sccm) into the chamber for 1 min, maintaining a substrate temperature of 800 °C. The reactor pressure was 30 Torr during all procedures.

The DLC layer was then deposited onto the VACNT surface using a plasma-enhanced CVD (PECVD) reactor fed with

hexane vapor and argon gas at 0.01−0.03 Torr for 10 min and a discharge voltage of −700 V.[24] Morphological analyses were performed with a high-resolution scanning electron microscope (FEI Inspect F50) operated at 20−30 kV. A Renishaw laser Raman spectrometer excited by an argon-ion laser (λ = 514.5 nm) provided the room temperature Raman spectra. The spot size was 15 μm and laser power was around 6 mW.

A parallel-plate configuration was used for field-emission measurements, with a sample acting as the cathode and a phosphor screen acting as the anode. A 10 nm gold or aluminum layer coated the anode to collect the current. A silica spacer kept a fixed separation of d = 150 μm between the two electrodes. The vacuum chamber pressure was 5×10^{-7} Torr. The emission current, I, was measured as the anode voltage, V, was ramped up and down under computer control. The phosphor screen emitted light when struck by the emitted electrons, and this allowed the emission area, A, to be estimated. To normalize the data, therefore, we have plotted emission current density, J (A cm^{-2}) versus electric field, E (V μm^{-1}), as well as in the form of a Fowler−Nordheim (F−N) plot ($\ln(J/E^2)$ versus $1/E$).[8]

3. RESULTS AND DISCUSSION

Figures 1a−f show typical SEM images of the VACNT forest and VACNT/DLC composite structures. Figure 1a shows the as-grown VACNT forest, and highlights its alignment, its high spatial density, and relatively flat, carpetlike surface.[25] The CNTs are ∼40 μm long and about 40 nm thick; with each CNT nearly touching its neighbor (separation distance is estimated at ∼10 nm. The top view of the VACNT/DLC sample shows a patterned surface (Figure 1b), indicating that after a few minutes of DLC deposition the VACNT tips have stuck together. Unlike with diamond CVD, however, instead of individual teepee structures the DLC coating has caused the CNTs to form linked rings, a bit like a honeycomb structure, although less regular. The type of microstructuring (teepees, honeycombs, or two-dimensional ridges) seen when depositing films onto CNTs depends mostly upon the density of CNT growth, and for these VACNTs the density was such that honeycomb structures predominate. On the crests of the honeycomb edges one can see a build-up of DLC, as shown in Figure 1c. Figure 1d shows details of the nanotubes before and after DLC deposition using high magnification TEM. Before deposition, the typical CNT diameter is 30−50 nm (consistent with image a), and after deposition the diameter is measured at 80−100 nm (inset), which suggests that the average DLC thickness on the CNT walls is ∼25 nm, although it may be considerably thicker than this on the top surface (as shown in Figure 1c).

In a separate experiment, some as-grown VACNT samples were wetted with a drop of water and dried at room temperature, see Figure 1e. The as-grown sample is hydrophobic and the drop of water caused the CNT tips to stick together to form honeycomb structures, although they are not as well-defined as in Figure 1b. The detail of the clustering at the tips of the CNTs can be seen in Figure 1f. Although honeycomb structures can be formed in VACNT forests by both DLC deposition (Figure 1b) and wetting (Figure 1e), the feature sizes are very different. The wetted VACNT forest has honeycomb structures ∼500 nm in size, whereas the VACNT/DLC honeycombs are ∼5 μm. Moreover, the honeycombs formed by wetting (Figure 1f) are only held together by contact forces (van der Waals forces), whereas those in Figure 1c are locked into shape because of the chemical bonding between the DLC coating and the underlying nanotubes. This suggests that the DLC layer locks the tips of the tubes together both chemically and physically.

Because the pulsed PECVD process contains hydrogen, the DLC it produces has properties consistent with those of hydrogenated amorphous carbon films (a-C:H).[3,10,21] The presence of H within the film changes the network by converting some C═C groups into sp^3-bonded −CH$_3$ groups.[26] Figure 2 shows typical Raman spectra of the

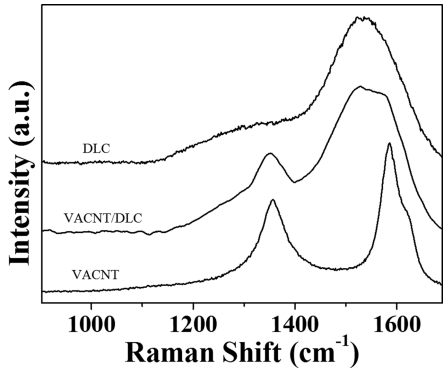

Figure 2. Raman spectra of the DLC film, the CNT forest, and the VACNT-DLC composite.

VACNT/DLC composite, the DLC film and the as-grown VACNT forest. The DLC spectrum shows two broad Gaussian bands, the D band centered at 1340 cm^{-1} resulting from the breathing mode of sp^2 carbon sites in rings but not chains, and the G band centered ∼1537 cm^{-1} arising from stretching of any pair of sp^2 sites whether in rings or chains. The intensity ratio I_D/I_G was used, together with suitable calibration graphs (see Figure 7 in ref 27) to estimate the sp^3 carbon content and the optical or Tauc band gap.[28,29] For the DLC film with an intensity ratio of I_D/I_G = 0.28, following this procedure gives an sp^3 carbon content of ∼60−70% and a Tauc gap of ∼2−2.5 eV. In the VACNT/DLC composite, I_D/I_G = 0.52, which corresponds to ∼45−55% sp^3 and Tauc gap ∼1.6−1.8 eV.

The VACNT first-order Raman spectrum (Figure 2) has two pronounced peaks centered at 1357 cm^{-1} (D-band) and 1585 cm^{-1} (G-band).[30,31] The D-band for CNTs is related to defects and disordered carbon, whereas the G-band (E_{2g}) is related to well-ordered crystalline graphite.[18,22] The D′-peak (1622 cm^{-1}) is also observed and is also correlated to disorder.[18] The VACNT second-order Raman spectrum revealed a pronounced G′-peak, confirming the good crystallinity shown by Figure 1d. The Raman spectrum of VACNT/DLC films is a combination of both DLC and VACNT Raman characteristics. Clearly, for VACNT/DLC the narrower VACNT D-band appears combined with the broader DLC one, and the G-band shows a broader feature involving the DLC G-band and the VACNT G- and D′-bands. This indicates that the DLC has not replaced the CNTs, but simply coated them.

Panels a and b in Figure 3 show the data from the field-emission measurements performed on 3 types of sample, the as grown VACNT forest, a wetted VACNT forest, and a DLC/VACNT composite. For this experiment we have defined the threshold field, E_{th}, as that corresponding to an electron emission density of 0.01 mA cm^{-2}. From the as-grown VACNT, E_{th} was ∼3.2 V μm^{-1}, consistent with previously published values for CNT arrays.[32,33] E_{th} for the wetted

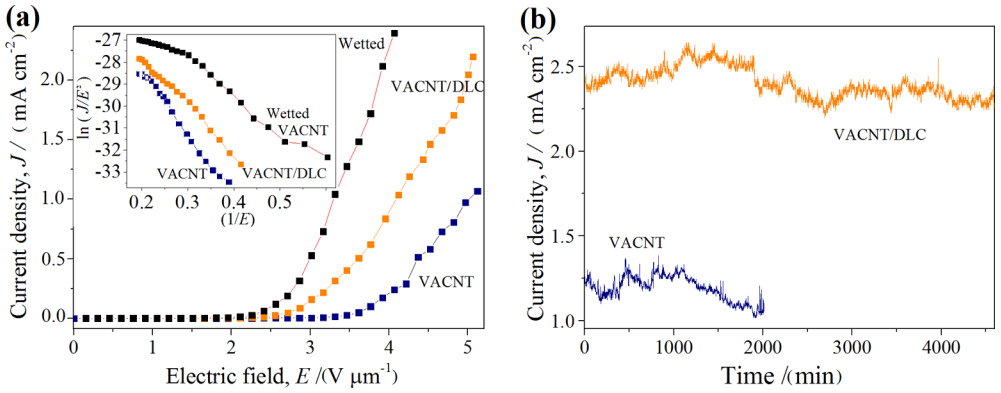

Figure 3. (a) Field-emission characteristics of the VACNT forest, the DLC-coated VACNT forest, and the wetted VACNT samples, showing curves of current density, *J*, versus electric field, *E*, for an average of 5 data sets. Inset: Fowler–Nordheim plots from the 3 types of samples. (b) Field-emission current–density stability test from the uncoated VACNT and VACNT/DLC samples.

VACNT decreased to ~1.8 V μm^{-1}, and for VACNT/DLC E_{th} ~2.1 V μm^{-1}. These data are all consistent with the F–N model for electron emission via quantum mechanical tunnelling through a potential barrier.[34] The field-enhancement factor β was calculated using the F–N equation

$$\ln\left(\frac{J}{E^2}\right) = \left(-\frac{b\phi^{3/2}}{\beta}\right)\left(\frac{1}{E}\right) + \ln(A\beta^2/\phi)$$

where J is the emission current density in A μm^{-2}, $b = 6.83 \times 10^3$ $eV^{-3/2}$ V μm^{-1}, $A = 1.56 \times 10^{-6}$ A V^{-2} eV, E is the applied electric field in V μm^{-1}, and ϕ is the work function of the material in eV. In the literature, the work function of DLC ranges from 1.5 to 4.7 eV,[35] depending on the type of amorphous carbon produced. In our case, using the calibration graph from Figure 10 in ref 34, our DLC film with a thickness of ~25 nm gives an sp^3 ratio of ~50% (consistent with the estimate made from Figure 1d) and a work function of ~4 eV. Consistent with previous authors, we have taken the work function of CNTs to be ~5.0 eV.[36]

The field-enhancement factor was then estimated by fitting the slope of the F–N plot (inset within Figure 3a) to $-b\phi^{3/2}/\beta$. The average field-enhancement factors obtained this way were $\beta \approx 2695$, 5277, and 2529 for as-grown VACNT, wetted VACNT, and VACNT/DLC samples, respectively, values that are consistent with those from other reports from similar patterned VACNT emitting systems.[37,38] Note that the geometrical β (~2000) calculated from (h/r) using the height (h) and radius (r) of the individual nanotubes is considerably lower than the values calculated from these F–N plots, a finding which is often reported for field-emission from VACNT forests.[32] There are a number of possible suggested reasons for this difference, including (a) perturbations of the electric field because of the experimental configuration, especially the interelectrode separation,[39] (b) the emission being a multistage process from many adjacent emitting tips rather than being from one isolated tip,[40] (c) electrical and thermal conduction effects from the surrounding VACNT forest,[36] and/or (d) high field enhancement at the nanotube–substrate–vacuum triple junction at the base of the CNTs causing electrons to be emitted directly into the vacuum.[32] Thus, it is clear that although the absolute magnitude of β values derived from F–N plots should be regarded with caution,[38] so long as they were measured under identical conditions then sensible deductions can be made based on their relative values.

For our results, the trend in the measured β values is consistent with the geometry and sharpness of the overall emitting structures.[41] The flattest sample is the as-grown VACNT forest while the sharpest is the wetted VACNT forest, and these have the lowest and highest β values, respectively. The VACNT/DLC composite can be thought of as a smoothed version of the latter, and has an intermediate β value. Furthermore, the emission current from the VACNT/DLC samples may have been higher than expected because of tunnelling of electrons from the CNT ends through the DLC capping layer, which is a relatively easy process because of the lower work function of DLC.

Stability tests performed on the same samples measured the emission current as a function of time maintaining the potential constant at 1700 V, as shown in Figure 3b. Visual observation of the bright area on the phosphor screen allowed the uniformity of the emission current within the emission area to be estimated. For all three samples, emission was uniform (i.e., uniform brightness on the phosphor screen) at the start of the test; however, as the test progressed, the three samples showed different behavior. The emission intensity from the wetted VACNT jumped between different spots, and the stability test was possible for no more than 100 min (which is why it is not plotted in Figure 3b). This behavior was probably due to the tip nanostructures separating because of heating during emission. For the VACNT sample, the field-emission current was uniform and constant throughout 20,000 min, but the current density used was quite low (1.25 mA cm^{-2}) and reduced substantially during the test due to the individual CNTs burning out. In contrast, the VACNT/DLC sample has a reasonably uniform emission current, but at a relatively high current density level (~2.2 mA cm^{-2}), and this continued for an uninterrupted period of 45 000 min. The test was halted only because the equipment was needed for another experiment, so the true lifetime could be much longer than this lower limit.

4. CONCLUSIONS

We have described a novel method to produce a low-cost, scalable, hybrid field-emission material by depositing DLC onto vertically aligned CNTs. Depending on the DLC deposition conditions and the CNT density, the hybrid structure develops nanostructuring whereby the CNT tips stick together to form honeycomb structures. Although there is only a small improvement in field-emission threshold voltage, the major

advantage of these hybrid structures is their significant improvement in emission current, lifetime, stability, and flickering characteristics. This hybrid material combines the excellent electrical conductivity and transport properties of multiple CNTs with the robust diamond-like surface of a DLC film with high sp^3 carbon content. The good electrical contact between the CNT and the titanium substrate may also contribute to the high currents achieved. Another contributing factor may be the physical separation of the honeycomb walls (typically 10−40 μm) which may help reduce space-charge effects that often limit emission current in more densely packed devices.

Although preliminary, these experiments have shown that such VACNT/DLC hybrids may be excellent candidates for a cheap, reliable, robust field-emission material. There are still a number of parameters that need to be investigated to improve and optimize the emission performance. These include the sp^2/sp^3 carbon ratio in the DLC, the conductivity of the DLC (which may be changed by doping with other elements), the size, length, and packing density of the CNTs, the substrate composition, the honeycomb separation, or alternative microstructures (teepees, ridges, etc.) that might be formed by changing the DLC deposition conditions.

■ ASSOCIATED CONTENT

Ⓢ Supporting Information

This material is available free of charge via the Internet at http://pubs.acs.org.

■ AUTHOR INFORMATION

Corresponding Author

*Phone: + 44 (0)117 928 7645. E-mail: hudson.zanin@bristol.ac.uk.

Notes

The authors declare no competing financial interest.

■ ACKNOWLEDGMENTS

We gratefully acknowledge the LME/LNLS-Campinas for microscopy support and mainly to Brazilian agency CNPq (202439/2012-7) for financial support. We also thank the School of Chemistry Electron Microscopy Unit for help with the SEM.

■ REFERENCES

(1) Umehara, Y.; Murai, S.; Koide, Y.; Murakami, M. *Diamond Relat. Mater.* **2002**, *11*, 1429−1435.
(2) Varshney, D.; Sumantc, A. V.; Resto, O.; Mendoza, F.; Quintero, K. P.; Ahmadi, M.; Weiner, B. R.; Morell, G. *Carbon* **2013**, *63*, 253−262.
(3) Sugie, H.; Tanemura, M.; Filip, V.; Iwata, K.; Takahashi, K.; Okuyama, F. *Appl. Phys. Lett.* **2001**, *78*, 2578−2580.
(4) Milne, W. I.; Teo, K. B. K.; Minoux, E.; Groening, O.; Gangloff, L.; Hudanski, L.; Schnell, J. P.; Dieumegard, D.; Peauger, F.; Bu, I. Y. Y.; Bell, M. S.; Legagneux, P.; Hasko, G.; Amaratunga, G. A. J. *J. Vac. Sci.Technol. B* **2006**, *24*, 345−348.
(5) Zou, R.; Hu, J.; Song, Y.; Wang, N.; Chen, H.; Chen, H.; Wu, J.; Sun, Y.; Chen, Z. *J. Nanosci. Nanotechnol.* **2010**, *10*, 7876−7896.
(6) Chen, G.; Shin, D. H.; Kim, S.; Roth, S.; Lee, C. J. *Nanotechnology* **2010**, *21*, 015704.
(7) Gröning, O.; Küttel, O. M.; Emmenegger, C.; Gröning, P.; Schlapbach, L. *J. Vac. Sci. Technol. B* **2000**, *18*, 665−678.
(8) Zou, Y.; May, P. W.; Vieira, S. M. C.; Fox, N. A. *J. Appl. Phys.* **2012**, *112*, 044903.
(9) Lay, J. H.; O'Donnell, K. M.; May, P. W. *Chem. Phys. Lett.* **2011**, *515*, 151−154.
(10) Orlanducci, S.; Guglielmotti, V.; Cianchetta, I.; Sessa, V.; Tamburri, E.; Toschi, F.; Terranova, M. L.; Rossi, M. *Nanosci. Nanotechnol. Lett.* **2012**, *4*, 338−343.
(11) Guglielmotti, V.; Tamburri, E.; Orlanducci, S.; Terranova, M. L.; Rossi, M.; Notarianni, M.; Fairchild, S. B.; Maruyama, B.; Behabtu, N.; Young, C. C.; Pasquali, M. *Carbon* **2013**, *52*, 356−362.
(12) Shrestha, S.; Choi, W. C.; Song, W.; Kwon, Y. T.; Shrestha, S. P.; Park, C.-Y. *Carbon* **2010**, *48*, 54−59.
(13) Lin, Z. D.; Young, S.-J.; Hsiao, C.-H.; Chang, S.-J.; Huang, C. S. *IEEE Photonics Technol. Lett.* **2013**, *25*, 1017−1019.
(14) Ho, Y. M.; Yang, G. M.; Zheng, W. T.; Wang, X.; Tian, H. W.; Xu, Q.; Li, H. B.; Liu, J. W.; Qi, J. L.; Jiang, Q. *Nanotechnol.* **2008**, *19*, 065710.
(15) Terranova, M. L.; Orlanducci, S.; Fiori, A.; Tamburri, E.; Sessa, V.; Rossi, M.; Barnard, A. S. *Chem. Mater.* **2005**, *17* (12), 3214−3220.
(16) Guglielmotti, V.; Chieppa, S.; Orlanducci, S.; Tamburri, E.; Toschi, F.; Terranova, M. L.; Rossi, M. *Appl. Phys. Lett.* **2009**, *95*, 222113.
(17) Trava-Airoldi, V. J.; Bonetti, L. F.; Capote, G.; Fernandes, J. A.; Blando, E.; Hubler, R.; Radi, P. A.; Santos, L. V.; Corat, E. J. *Thin Solid Films* **2007**, *516*, 272−276.
(18) Marciano, F. R.; Bonetti, L. F.; Lima-Oliveira, D. A.; Mello, C. B.; Ueda, M.; Corat, E. J.; Trava-Airoldi, V. J. *Diamond Relat. Mater.* **2010**, *19*, 1139−1143.
(19) Karabutov, A. V.; Konov, V. I.; Ralchenko, V. G.; Obraztsova, E. D.; Frolov, V. D.; Uglov, S. A.; Scheibe, H. J.; Strelnitskij, V. E.; Polyakov, V. I. *Diamond Relat. Mater.* **1998**, *7*, 802−806.
(20) Huq, S. E.; Prewett, P. D.; She, J. C.; Deng, S. Z.; Xu, N. S. *Mater. Sci. Eng., B* **2000**, *74*, 184−187.
(21) Gröning, O.; Küttel, O. M.; Gröning, P.; Schlapbach, L. *Appl. Surf. Sci.* **1997**, *111*, 135−139.
(22) May, P. W.; Hohn, S.; Wang, W. N.; Fox, N. A. *Appl. Phys. Lett.* **1998**, *72*, 2182−2184.
(23) Zanin, H.; Saito, E.; Ceragioli, H. J.; Baranauskas, V.; Corat, E. J. *Mater. Res. Bull.* **2014**, *49C*, 487−493.
(24) Wachesk, C. C.; Pires, C. A. F.; Ramos, B. C.; Trava-Airoldi, V. J.; Lobo, A. O.; Pacheco-Soares, C.; Marciano, F. R.; Da-Silva, N. S. *Appl. Surf. Sci.* **2013**, *266*, 176−181.
(25) Antunes, E. F.; Lobo, A. O.; Corat, E. J.; Trava-Airoldi, V. J. *Carbon* **2007**, *45*, 913−921.
(26) Irmer, G.; Dorner-Reisel, A. *Adv. Eng. Mater.* **2005**, *7*, 694−705.
(27) Ferrari, A. C.; Robertson, J. *Philos. Trans. R. Soc. London, Ser. A* **2004**, *362*, 2477−2512.
(28) Tamor, M. A.; Vassell, W. C. *J. Appl. Phys.* **1994**, *76*, 3823−3830.
(29) Ferrari, A. C.; Robertson, J. *Phys. Rev.* **2000**, *B61*, 14095−14107.
(30) Tsukada, J.; Zanin, H.; Barbosa, L. C. A.; da Silva, G. A.; Ceragioli, H. J.; Peterlevitz, A. C.; Teofilo, R. F.; Baranauskas, V. *J. Electrochem. Soc.* **2012**, *159*, D159−D161.
(31) Zanin, H. G.; Peterlevitz, A. C.; Teofilo, R. F.; Ceragioli, H. J.; Baranauskas, V. *Ferroelectrics* **2012**, *436*, 96−100.
(32) Asli, N. A.; Shamsudin, M. S.; Falina, A. N.; Azmina, M. S.; Suriani, A. B.; Rusop, M.; Abdullah, S. *Microelectron. Eng.* **2013**, *108*, 86−92.
(33) Chhowalla, M.; Ducati, C.; Rupesinghe, N. L.; Teo, K. B. K.; Amaratunga, G. A. J. *Appl. Phys. Lett.* **2001**, *79*, 2079−2081.
(34) Chen, G.; Neupane, S.; Li, W.; Chen, L.; Zhang, J. *Carbon* **2013**, *52*, 468−475.
(35) Evtukh, A. A.; Hartnagel, H.; Litovchenko, V. G.; Semenenko, M. O.; Yilmazoglu, O. *Semicond. Sci. Technol.* **2004**, *19*, 923−929.
(36) de Jonge, N.; Allioux, M.; Doytcheva, M.; Kaiser, M.; Teo, K. B. K.; Lacerda, R. G.; Milne, W. I. *Appl. Phys. Lett.* **2004**, *85*, 1607−1609.
(37) Tsai, T. Y.; Lee, C. Y.; Tai, N. H.; Tuan, W. H. *Appl. Phys. Lett.* **2009**, *95*, 013107.
(38) Li, C.; Zhang, Y.; Mann, M.; Hasko, D.; Lei, W.; Wang, B.; Chu, D.; Pribat, D.; Amaratunga, G. A. J.; Milne, W. I. *Appl. Phys. Lett.* **2010**, *97*, 113107.

(39) Bonard, J. M.; Croci, M.; Arfaoui, I.; Noury, O.; Sarangi, D.; Châtelain, A. *Diamond Relat. Mater.* **2002**, *11*, 763−768.
(40) Huang, J. Y.; Kempa, K.; Jo, S. H.; Chen, S.; Ren, Z. F. *Appl. Phys. Lett.* **2005**, *87*, 053110.
(41) Zuo, Y.; Ren, Y.; Wang, Z.; Han, X.; Xi, L. *Org. Electron.* **2013**, *14*, 2306−2314.